IVYSPRING INTERNATIONAL PUBLISHER

Theranostics

2016; 6(1): 40-53. doi: 10.7150/thno.13250

Research Paper

Hyaluronic Acid Modified Hollow Prussian Blue Nanoparticles Loading 10-hydroxycamptothecin for Targeting Thermochemotherapy of Cancer

Lijia Jing [1], shangmin shao [3],Yang Wang [3],Yongbo Yang[1], Xiuli Yue [1]✉, Zhifei Dai [2]✉

1. State Key Laboratory of Urban Water Resources and Environment, School of Life Science and Technology, Harbin Institute of Technology, Harbin 150080, China
2. Department of Biomedical Engineering, College of Engineering, Peking University, Beijing 100871, China.
3. Alkali Soil Natural Environmental Science Center, Northeast Forestry University; Key Laboratory of Saline-alkali Vegetation Ecology Restoration in Oil Field, Ministry Education, Harbin, 150040, China

✉ Corresponding authors: Xiuli Yue, Email: xiulidx@163.com, Zhifei Dai, Email: zhifei.dai@pku.edu.cn

Received: 2015.07.15; Accepted: 2015.08.28; Published: 2016.01.01

Abstract

This paper reported the fabrication of a multifunctional nanoplatform by modifying hollow Prussian blue nanoparticles with hyaluronic acid grafting polyethylene glycol, followed by loading 10-hydroxycamptothecin for tumor-targeted thermochemotherapy. It was found that the surface modification of hollow Prussian blue nanoparticles with hyaluronic acid grafting polyethylene endowed a great colloidal stability, long blood circulation time and the capability for targeting Hela cells over-expressing the CD44 receptor. The obtained nanoagent exhibited efficient photothermal effect and a light triggered and stepwise release behavior of 10-hydroxycamptothecin due to the strong optical absorption in the near-infrared region. The investigations on the body weight change, histological injury and blood biochemical indexes showed that such nanoagent had excellent biocompatibility for medical application. Both in vitro and in vivo experiments proved that the combination of chemotherapy and photothermal therapy through the agent of hyaluronic acid modified Prussian blue nanoparticles loading 10-hydroxycamptothecin could significantly improve the therapeutic efficacy compared with either therapy alone because of a good synergetic effect.

Key words: Prussian blue; Hyaluronic acid; 10-hydroxycamptothecin; Chemotherapy; Photothermal therapy

Introduction

Chemotherapy has been widely used for cancer treatment. Despite the major benefits, patients receiving chemotherapeutic treatment usually experience side effects. The dose of drug required to achieve clinically effective cytotoxicity in tumors often causes severe damage to actively propagating nonmalignant cells. To overcome these problems, various drug delivery strategies with lower systemic toxicity and better drug cell internalization than free drug have been proposed [1-7]. However, it is not easy to achieve the spatial and temporal control of local drug release in many clinical applications. The light-triggered drug release has attracted intensive research interests since it may allow for precise, on-demand drug delivery within individual cells in vitro or, may enable precise treatment of cancer in vivo [8, 9].

Photothermal therapy (PTT) employing photothermal agent and near infrared (NIR) laser for thermal ablation of tumor provides a minimally invasive methodology for cancer treatment [10-15]. Yet, PTT alone is challenged to completely eradicate tumor because of the insufficient tumor-target specificity of PTT agents and the suboptimal laser energy in deep tissue due to light scattering and absorption [9]. Co-administration of multiple therapeutic modalities

has been an increasingly important strategy in medicine. For example, tumor-selective thermochemotherapy through exogenous laser irradiation is becoming increasingly attractive for its remarkable spatial/temporal resolution since hyperthermia increases cellular metabolism and membrane permeability for enhanced drug uptake [16-20]. However, simple co-injection/ingestion of multiple drugs, such as photothermal agent and chemical drugs, fails to normalize their pharmacokinetic and pharmacodynamics properties and hardly allow them to reach the same target for combinatory effects. Nevertheless, it is an obvious, significant, and unique advantage to integrate photothermal agents and anti-cancer drugs through a single nanoplatform with rationally designed doses, prolonged circulation, selective/targeted accumulation and stimuli-responsive drug release/activation [21-25]. In that case, PTT and chemotherapy could be simultaneously applied to cancerous tumor to exert their synergistic effect, offering both rapid tumor ablation and long-term tumor resistance, leading to significantly improved therapeutic efficacy.

To date, a variety of photothermal agents such as carbon and metal-based nanomaterials have been successfully explored [26-34]. However, most of the reported photothermal agents are far from clinical application due to their unpredictable metabolic pathways and potential long-term toxicity in vivo [35, 36]. Prussian blue (PB) is a clinical drug approved by U.S. Food and Drug Administration (FDA) for treating the radioactive exposure of thallium and cesium [37]. Recently, PB has been explored as a new generation of photothermal agent for ablation of cancerous tumor due to the strong absorption and excellent photothermal conversion efficiency in the NIR region in our group [38-40]. PB nanoparticles take more advantages for PPT treatment due to its low cost, outstanding photothermal stability and, most importantly, the FDA approved security for clinical applications. Especially, hollow PB nanoparticles are of interest due to their potential for encapsulation of large quantities of guest molecules or large-sized guests within their empty core domain[41, 42].

This paper describe the development of a multifunctional nanoagent by integrating different components including hollow PB nanoparticle as photothermal agent and drug carrier, 10-hydroxycamptothecin (HCPT) as chemotherapeutic agent, and hyaluronic acid grafting polyethylene glycol (HA-g-PEG) as capping agent for prolonged blood circulation time and CD44 receptor mediated tumor targeting into one single agent. HCPT is a natural pentacyclicindole alkaloid which was extracted from a Chinese tree, *Camptothecaacuminata* Decne and showed good activities against gastric carcinoma, hepatoma, leukemia and tumor of head and neck[43]. HA is a specific ligand that binds CD44 receptor, a transmembrane glycoprotein overexpressed in a variety of cancer cells [44, 45]. Inspired by this finding, HA has been widely investigated and successfully utilized as an efficient cancer targeting moiety for tumor-targeted diagnostic and therapeutic applications [46-49]. The physicochemical properties of the nanoagent including morphology, size distribution, photothermal capability, drug loading efficiency and drug release behavior were characterized. The in vitro and in vivo tumor targeting and anticancer activities were evaluated using human cervical cell line (Hela cells) and Hela tumor bearing mice.

Materials and methods

Chemicals

$K_3[Fe(CN)_6]$ and poly(vinylpyrrolidone) (PVP, K30) were obtained from Sinopharm Chemical Reagent Co., Ltd. Poly (allylamine hydrochloride) (PAH, MW=56k), IRDye® 800CW NHS Ester was purchased from LI-COR Biosciences. 1-(3-Dimethylaminopropyl)-3-ethylcarbodiimide hydrochloride (EDC), N-Hydroxysuccinimide (NHS) and Poly(acrylic acid) (PAA, MW=18k), 3,8-Diamino-5-[3-(diethylmethylammonio)propyl]-6-pheny-lphenanthridinium diiodide (PI), 3,6-Di(O-acetyl)- 4,5-bis[N,N-bis(carboxymethyl)-aminomethyl]fluorescein, tetraacetoxymethyl ester (Calcein-AM) and 3-(4,5-dimethylthiazol-2-yl)-2,5-diphenyltetrazolium bromide (MTT) were obtained from Sigma-Aldrich. Hyaluronic acid (HA, MW=32k) was obtained from Zhenjiang Dong Yuan Biotechnology Corporation (zhenjiang, China). Carboxyl-terminated methoxypoly (ethyleneglycol) (mPEG-COOH, MW=35k) was obtained from Kaizheng Biotechnology Corporation (beijing, China). 10-hydroxycamptothecin (HCPT) was obtained from Harbin Foran High-Tech Development Ltd. (Harbin, Heilongjiang, China). All other chemicals and reagents were of analytical grade. All the aqueous solutions were prepared with deionized water (18.2 MΩ cm) from a Milli-Q purification system.

Fabrication of hollow Prussian blue nanoparticles (HPBNs)

PVP coated hollow Prussian blue nanoparticles (HPBNs) were fabricated according to the reported procedure with some modifications [50]. Firstly, 3 g of PVP and 110 mg of K_3 [$Fe(CN)_6$] were dissolved into 40 mL of HCl solution (0.01M) under magnetic stirring. The clear solution was then placed into a reaction kettle and heated at 80 ^oC for 24 h. Afterwards, PVP coated solid PB nanoparticles were obtained by

centrifugation and washed with DI water and ethanol three times. Then, solid PB nanoparticles (20 mg) and PVP (100 mg) were dissolved in 20 mL of HCl solution (1.0 M) under magnetic stirring. After stirring for 2 h, the solution was transferred into a reaction kettle and heated at 140 ^{o}C for 4 h. After acid etching, PVP coated hollow PB nanoparticles were obtained by centrifugation and washed with DI water and ethanol three times.

Synthesis of hyaluronic acid grafting polyethylene glycol (HA-g-PEG)

Briefly, 500mg of mPEG-NH_2 and 1g of HA were dissolved in 20 mL of N, N-dimethylformamide (DMF), followed by adding 100mg of EDC and 50mg of NHS. The reaction was allowed overnight at room temperature under the protection of nitrogen. Then, the resulting solution was concentrated under reduced pressure and dialyzed in DI water using dialysis bag (molecular weight cut-off 12,000–14,000). Finally, the HA-g-PEG was obtained after lyophilization using a freeze dryer (TFD5505, Ilshin Lab, Korea). Chemical structure was analyzed by ^{1}H-NMR spectroscopy (**Figure S1**).

Synthesis of the HA-g-PEG and PEG modified HPBNs

In this step, both HA-g-PEG modified HPBNs and PEG modified HPBNs were fabricated according to the reported method with some modifications [40]. For fabricating HA-g-PEG modified HPBNs, 5 mL (2 mg/mL) of HPBNs was dropwise added into 10 mL PAA solution (3 mg/mL) slowly under ultrasonication. After further stirring for 3 h, a HPBNs@PAA solution was obtained after the removal of excess PAA molecules using filters (100 kDa MWCO, Millipore). Then, the obtained HPBNs/PAA solution was added dropwise into 20 mL PAH solution (3 mg/mL) under ultrasonication and then stirred for further 4 h. After the removal of excess PAH molecules using filters, the pH value of the solution was adjusted to be 7.4. Then, 1mL EDC solution (2 mg/mL) was dropwise added within 1h under vigorous stirring. The reaction was allowed overnight to induce chemical crosslinking between the carboxyl groups of PAA and the amino groups of PAH on the surface of HPBNs, and the resulted HPBNs@PAA/PAH were purified through filters. Finally, the obtained HPBNs@PAA/PAH solution was mixed 10 mL of HA-g-PEG solution (2 mg/mL in phosphate buffer) under sonication, followed by slowly adding 1 mg EDC into the mixture. Allowed for reaction overnight at room temperature, HPBNs@PAA/PAH/HA-g-PEG was obtained after the removal of excess HA-g-PEG molecules using filters (100 kDa, MWCO).

For fabricating PEG modified NPBNs, the above mentioned HPBNs@PAA/PAH solution was mixed 10 mL of mPEG-COOH solution (2 mg/mL in phosphate buffer) under sonication, followed by slowly adding 1 mg EDC into the mixture. The reaction was allowed overnight at room temperature, then HPBNs@PAA/PAH/PEG was obtained after the removal of excess mPEG-COOH molecules using filters (100 kDa, MWCO).

Characterization

The structure of the nanoparticles at different fabrication stages was imaged using transmission electron microscope (TEM). The size distributions and zeta potentials were evaluated by a 90Plus/BI-MAS instrument (Brookhaven Instruments Co., U.S.A). The UV/Vis/NIR absorption spectra were measured by a Varian 4000 UV-Vis spectrophotometer. The content of PB was evaluated using inductively coupled plasma optical emission spectrometry (ICP-OES).

Drug loading and release

For loading HCPT into HPBNs@PAA/PAH/HA-g-PEG, 10 mg of HCPT and 50 mg of HPBNs@PAA/PAH/HA-g-PEG were dispersed in 1 mL of dimethyl sulfoxide (DMSO). After magnetic stir of the dispersion at room temperature for 24 h, the HCPT loaded HPBNs@PAA/PAH/HA-g-PEG NPs (HCPT@HPBNs@PAA/PAH/HA-g-PEG) were obtained by centrifugation and washed with phosphate buffered saline (PBS) (10 mM, pH 7.4) three times. The loading content of HCPT was determined using a fluorescence spectrophotometer (Varian Cary Eclipse).

To investigate the HCPT release pattern under the physiological condition, 2 mg of HCPT@HPBNs@PAA/PAH/HA-g-PEG was suspended in 2 mL of PBS solution, sealed in dialysis bag and immersed in 20 mL of PBS solution. The amount of released HCPT was monitored at regular time intervals. The NIR-triggered release behavior of HCPT from HCPT@HPBNs@PAA/PAH/HA-g-PEG was investigated by treating 3 mL PBS solution of HCPT@HPBNs@PAA/PAH/HA-g-PEG with three cycles of laser on/off using a 808 nm NIR laser at an output power at 1.5 W (10 min for laser on, 50 min for laser off).

Photothermal potential of HCPT@HPBNs@PAA/PAH/HA-g-PEG

The photothermal effect was investigated by irradiating HCPT@HPBNs@PAA/PAH/HA-g-PEG solutions at different concentrations with a continuous-wave diode NIR laser (808 ± 10 nm, 1.5 W) for 10 min. The temperature was recorded by a digital

thermometer every 10 seconds. DI water was investigated for comparison.

Cellular experiment

Hela cells with high CD44 receptor expression were cultured in RPMI-1640 medium with 10% heat-inactivated fetal bovine serum, penicillin (100 U/mL), and streptomycin (100 mg/mL) at 37 °C and 5% CO_2. For comparative study of cellular uptake, Hela cells were incubated with the two drug free carriers of HPBNs@PAA/PAH/HA-g-PEG and HPBNs@PAA/PAH/PEG with different PB concentrations in 6 well-plate (2.0 mL per well) for 4 h, respectively. After washed with PBS three times, Hela cells were digested and counted. The uptake efficiency of the two kinds of NPs was evaluated by measuring the iron level using ICP-OES, respectively. To further study the cellular uptake, Hela cells were seeded in 6-well plates and incubated with HPBNs@PAA/PAH/HA-g-PEG and HPBNs@PAA/PAH/PEG at the same PB concentrations concentration of 150 μg/mL (dissolved in fresh medium) for 4 h at the environment of 37 °C and 5% CO_2. Afterwards, the cells were washed with PBS (pH 7.4) for observation on a fluorescence microscope (Leica, Germany).To visualize the photothermal cytotoxicity, Hela cells were incubated with HPBNs@PAA/PAH/HA-g-PEG and HPBNs@PAA/PAH/PEG with the same PB concentration (0.1 mg/mL) in 6 well-plate (2.0 mL per well) for 4 h. After washed with PBS three times, Hela cells were exposed to NIR laser (1 W/cm^2) for 10 min and then stained with calcein AM and PI, respectively. For further investigation on the cytotoxicity by various treatments, viability of the cells was measured by standard MTT method at a wavelength of 490 nm.

NIR fluorescence imaging

50 μg of IRDye® 800CW NHS Ester was firstly reacted with 100 mg of HPBNs@PAA/PAH in 5mL PBS under mechanical stirring over night. IRDye® 800CW labeled HPBNs@PAA/PAH was obtained after washed with PBS three times. Afterwards, 40mg of IRDye® 800 CW labeled HPBNs@PAA/PAH was reacted with 100 mg of HA-g-PEG and mPEG-COOH to form IRDye® 800CW labeled HPBNs@PAA/PAH/HA-g-PEG and HPBNs@PAA/PAH/PEG, respectively.

NIR fluorescence imaging was performed on IVIS Imaging Spectrum System (PerkinElmer, USA) and analyzed by IVIS Living Imaging 3.0 software. The tumor bearing nude mice were divided into two groups and intravenously injected with IRDye® 800CW labeled HPBNs@PAA/PAH/HA-g-PEG and HPBNs@PAA/PAH/PEG at the same PB dosage of 10 mg/kg (injection volume: 0.1 mL), respectively. The NIR fluorescence images were obtained at different time points. After 24h post-injection, the mice were sacrificed to investigate the fluorescence intensity of the blood and vital organs including heart, liver spleen, lung and brain. All animal procedures were in agreement with institutional animal use and care committee and carried out ethically and humanely.

Elimination of the NPs from the circulation

Health mouse were intravenously injected with HPBNs, HPBNs@PAA/PAH/PEG and HPBNs@PAA/PAH/HA-g-PEG NPs at the same PB dose of 10 mg/kg and blood samples (0.2 mL) were collected at different time. The pharmacokinetic parameters of the NPs in bloodstream were finally evaluated by measuring the Fe content in blood via ICP measurements after decomposing the blood samples by aqua regia. All the animal experiments were approved by institutional animal use committee and carried out ethically and humanely.

Animal experiments

Subcutaneous tumors were created by subcutaneous injection of 5×10^6 Hela cells in 100 μL PBS buffer onto the back of each mouse. The mice with similar tumor volumes about 100mm^3 were divided into several groups (n = 7), including the therapy groups and control groups. For PTT treatment, the 808 nm NIR laser was used at the power density of 1 W/cm^2 for 10 min. Tumor volume were recorded and calculated according to the formula: (tumor length) × (tumor width) ^{2}/2.

The toxicity of HCPT@HPBNs@PAA/PAH/HA-g-PEG was evaluated on health nude mice. After intravenous injection of HCPT@HPBNs@PAA/PAH/HA-g-PEG, body weights of the mice were recorded during 30 days. In addition, several mice were sacrificed at different time points. Blood and major organs including heart, liver, spleen lung and kidney were collected for blood biochemistry assay and histopathology investigation, respectively. Untreated nude mice were used as control.

Statistical Analysis

Statistical analyses were performed using Micorcal™ Origin 8.0 (Microcal Software). The results between the different materials were compared using one-way analysis of variance (ANOVA) (*$p < 0.05$ and **$p < 0.01$).

Results and Discussion

Preparation and characterization

The engineering procedure of HCPT@HPBNs@PAA/PAH/HA-g-PEG NPs was

illustrated in **Figure 1**. PVP coated Prussian blue nanoparticles were etched by using hydrochloric acid process, followed by alternative adsorption of PAA and PAH around the surface of the resulted HPBNs via the electrostatic layer-by-layer (LBL) self-assembly approach in combination of chemical crosslinking method. Finally, HA-g-PEG was conjugated onto the nanoparticle surface to ensure good colloidal stability and active tumor targeting.

The zeta potential and size distribution of nanoparticles at different fabrication stages were measured. As shown in **Figure 2A**, the zeta potentials decreased from about 8 mV for HPBNs to -21 mV for HPBNs/PAA due to the attachment of negatively charged PAA onto the surface of HPBNs, and then converted to +28 mV after adsorption of PAH, suggesting the successful self-assembly of PAA and PAH layers onto the NPs surface. After conjugating HA-g-PEG, the resulting HPBNs@PAA/PAH/HA-g-PEG NPs possessed a zeta potential of -17 mV due to the negative charge of the carboxylic groups in HA-g-PEG molecules. The dynamic light scattering (DLS) measurements showed that the nanoparticle sizes increased along with the assembly process. The average hydrodynamic diameter was found to be 84.68 ± 4.37 for HPBNs, 93.44 ± 6.89 nm for HPBNs@PAA, 105.21 ± 7.12 nm for HPBNs@PAA/PAH and 119.76 ± 6.57 for HPBNs@PAA/PAH/HA-g-PEG NPs. The appropriate and uniform size met the requirements of enhanced permeability and retention (EPR) effect in tumor vasculature, favoring the active targeting effect to cancer cells.

As photothermal agents for PTT, the property of strong optical absorption in the NIR region is essential. As shown in **Figure 2B**, the UV-vis absorption spectrum of HPBNs@PAA/PAH/HA-g-PEG NPs exhibited an abroad absorption band in the NIR region from 600 nm to 900 nm with a absorption peak around 700 nm, indicating that HPBNs@PAA/PAH/HA-g-PEG NPs could be used as a potential photothermal agent for PTT treatment of cancer.

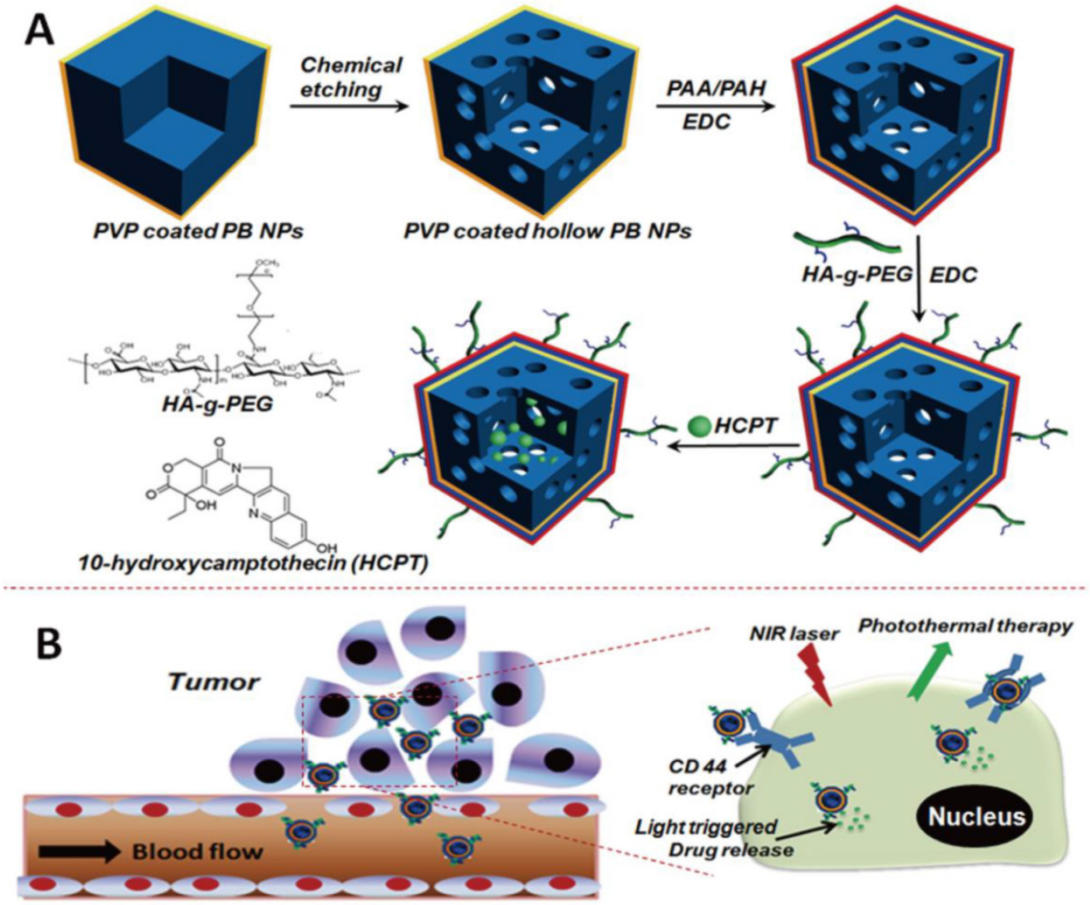

Figure 1. Engineering procedure (A) and functional description (B) of hyaluronic acid grafting polyethylene glycol modified hollow Prussian blue nanoparticles loading 10-hydroxycamptothecin for tumor-targeted thermochemotherapy.

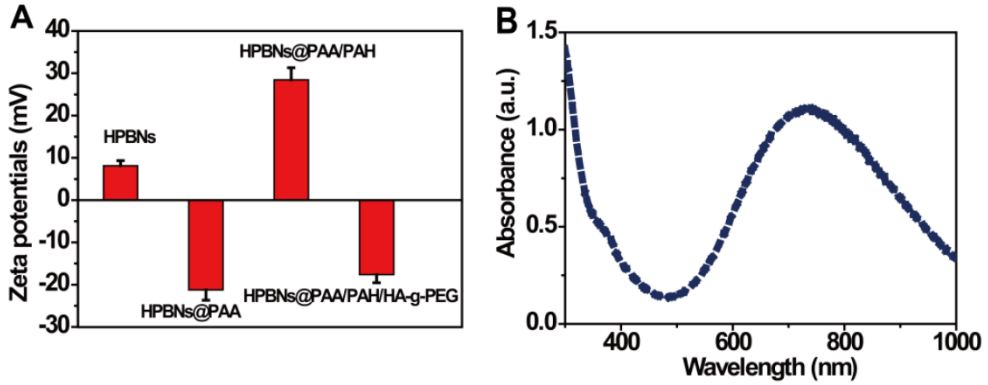

Figure 2. (A) Zeta potentials of the nanoparticles at different fabrication stages: HPBNs, HPBNs@PAA, HPBNs@PAA/PAH and HPBNs@PAA/PAH/HA-g-PEG NPs. (B) UV/vis absorption spectrum of HPBNs@PAA/PAH/HA-g-PEG NPs.

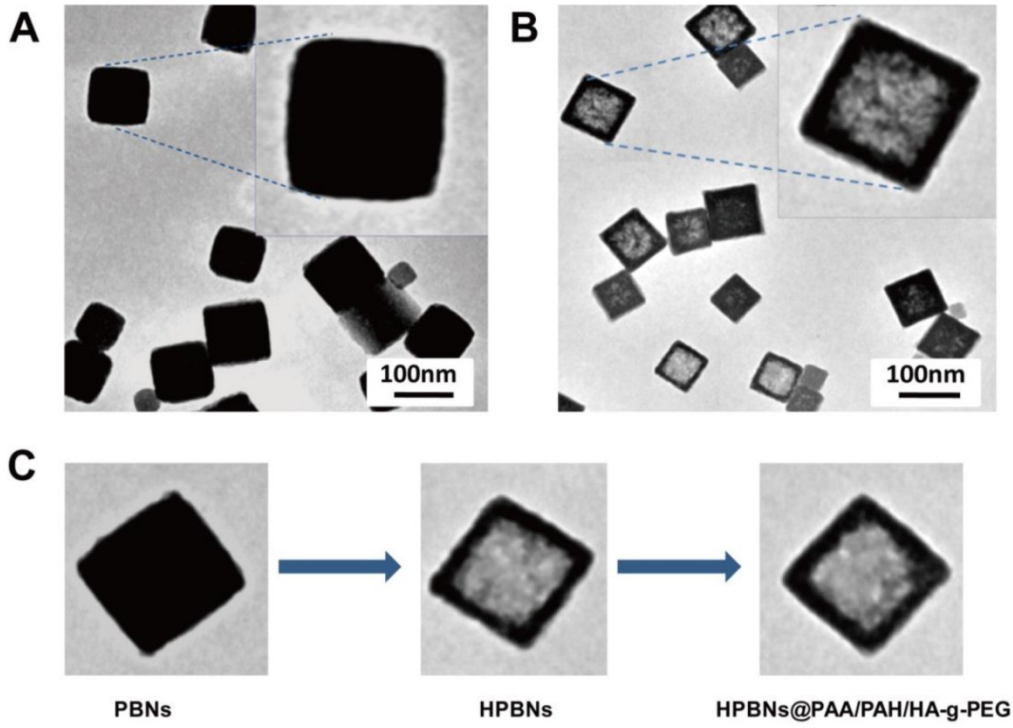

Figure 3. TEM image: (A) Solid Prussian blue nanoparticles; (B) HPBNs@PAA/PAH/HA-g-PEG NPs; (C) Nanoparticles at different fabrication stages.

TEM images confirmed that the HPBNs@PAA/PAH/HA-g-PEG NPs kept the cubical shape of the templating solid PB nanoparticles (**Figure 3**). They are uniform and well dispersed. Different from the solid PB nanoparticles, HPBNs@PAA/PAH/HA-g-PEG NPs possessed apparent cubical interior hollow cavities. N_2 adsorption–desorption isotherm of HPBNs@PAA/PAH/HA-g-PEG NPs was measured. As shown in **Figure S2**, compared with solid PB nanoparticles with BET surface area of 231 $m^2 \cdot g^{-1}$, HPBNs@PAA/PAH/HA-g-PEG NPs exhibited a steeply increased BET surface area of 398 $m^2 \cdot g^{-1}$ at very low relative pressure, indicating the formation of mesopores in the nanoparticles. The range of pore-size was from 1.9 nm to 7.8 nm.

Drug loading and passive drug release

Due to the sufficient interior hollow cavity for loading drug and the mesoporous channels in the surface for controlled drug release, HPBNs@PAA/PAH/HA-g-PEG NPs can be operated as an excellent drug delivery platform. The model drug of HCPT was readily loaded into HPBNs@PAA/PAH/HA-g-PEG NPs through a solvent exchange method. When the mass ratio of HCPT to HPBNs@PAA/PAH/HA-g-PEG NPs was 1:5, the drug-encapsulation efficiency (EE) was evaluated to be 52% and the loading content (LC) was up to 10.4%. As shown in **Figure 4A**, the resulted HCPT@HPBNs@PAA/PAH/HA-g-PEG NPs processed an excellent long-term colloidal stability in

plasma due to the introduction of PEG, which could take advantage to avoid the removal by the reticuloendothelial system, increasing the blood circulation time in vivo.

The release pattern of HCPT from HCPT@HPBNs@PAA/PAH/HA-g-PEG NPs was investigated at physiologic condition (37°C, pH 7.4). As seen from **Figure 4B**, only about 33 % of HCPT was released from the HCPT@HPBNs@PAA/PAH/HA-g-PEG NPs within 48h. This slow release rate from HCPT@HPBNs@PAA/PAH/HA-g-PEG NPs was attributed to a slow exchange rate between the inner loading drug and the external aqueous medium through the mesoporous channels in the nanoparticle. Such slow passive drug release rate at physiologic condition is advantageous to minimize the toxic and side effect in health tissue by avoiding burst release. Furthermore, it may ensure the high drug accumulation in cancerous tumor although it may take time for tumor cells to take up the nanoagents.

Photothermal effect and triggered drug release

Aqueous dispersions of HCPT@HPBNs@PAA/PAH/HA-g-PEG NPs at different concentrations were exposed to an 808 nm NIR laser at the output power of 1.5 W to investigate the photothermal capability. **Figure 4C** showed the temperature elevations of different samples during the NIR laser irradiation. It was found that HCPT@HPBNs@PAA/PAH/HA-g-PEG NPs exhibited dramatically elevated temperature during the irradiation of NIR laser. In comparison, no significant temperature elevation was observed in the case of DI water, verifying the excellent photothermal conversion efficiency of HCPT@HPBNs@PAA/PAH/HA-g-PEG NPs. In addition, the temperature elevation amplitude increased obviously with the increasing concentration of HCPT@HPBNs@PAA/PAH/HA-g-PEG NPs. The nanoagent at the concentration of 0.1 mg/mL and 0.2 mg/mL achieved temperature elevation of 18.0 °C and 24.1 °C, respectively. It is worth noting that irradiation of the nanoagent at 0.1 mg/mL for only 4 min can achieve a temperature elevation of 11.2 °C. It is sufficient for thermal ablation of cancer cells in vivo, suggesting the high potential for in vivo PTT treatment of cancer.

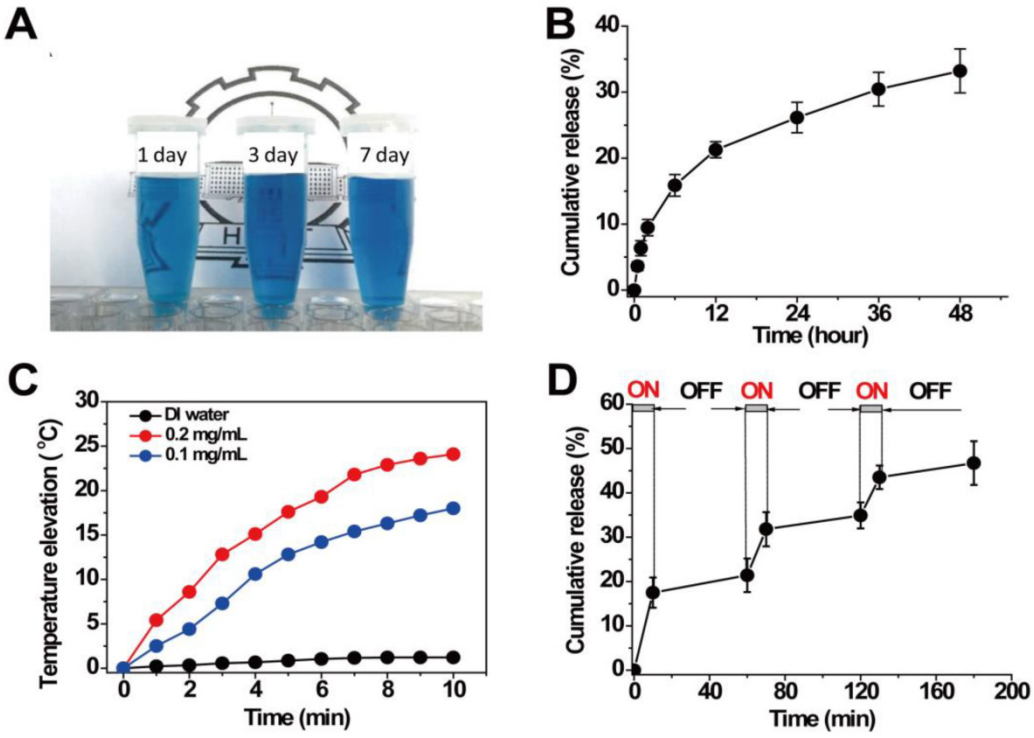

Figure 4. (A) HCPT@HPBNs@PAA/PAH/HA-g-PEG NPs suspended in plasma for different time; (B) In vitro release pattern of HCPT from HCPT@HPBNs@PAA/PAH/HA-g-PEG NPs at 37°C and pH 7.4; (C) Temperature elevations of HCPT@HPBNs@PAA/PAH/HA-g-PEG NPs at different concentrations under NIR laser irradiation (808 nm, 1.5 W); (D) HCPT release profile from HCPT@HPBNs@PAA/PAH/HA-g-PEG NPs with three cycles of laser on/off. All release studies were performed in triplicate.

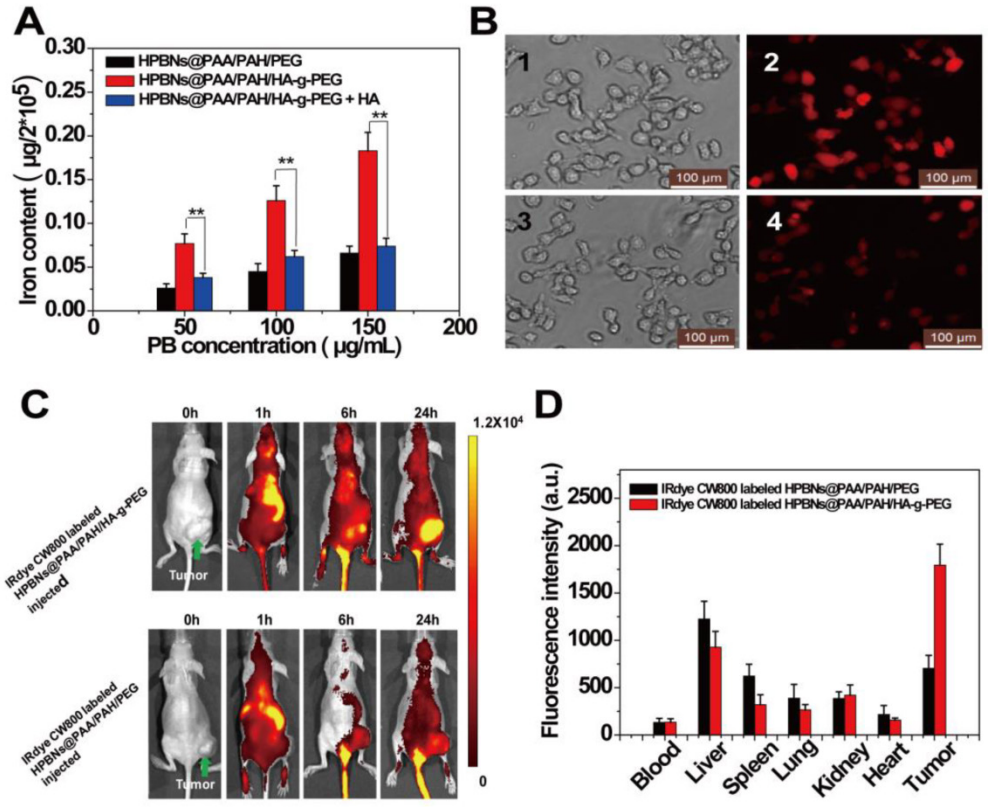

Figure 5. (A) Iron content in Hela cells after incubated with HPBNs@PAA/PAH/PEG, HPBNs@PAA/PAH/HA-g-PEG and HPBNs@PAA/PAH/HA-g-PEG + free HA. (B) Fluorescence microscopy images of Hela cells after incubation with HPBNs@PAA/PAH/PEG and HPBNs@PAA/PAH/HA-g-PEG and at the PB concentration of 150 μg/mL for 4h: bright field image (1) and fluorescence image (2) of HPBNs@PAA/PAH/HA-g-PEG treated Hela cells, bright field image (3) and fluorescence image (4) of HPBNs@PAA/PAH/PEG treated Hela cells. (C) Fluorescence images of mice bearing Hela tumor at different time points after intravenous injection of IRdye CW800 labeled HPBNs@PAA/PAH/HA-g-PEG and HPBNs@PAA/PAH/PEG, respectively. (D) Fluorescence intensity of tumor and main organs in tumor bearing mice after 24 h injection of above two different NPs, respectively. **: $p < 0.01$.

The release pattern of HCPT under laser irradiation was evaluated by repeatedly irradiating HCPT@HPBNs@PAA/PAH/HA-g-PEG NPs over a period of 10 min, followed by 50 min intervals with the laser turned off. A rapid release rate of HCPT was observed during each laser irradiation and the drug release rate slowed down when the laser was switched off (**Figure 4D**). With three cycles of laser on/off treatment, the percentage release of HCPT increased to 47.2 % within 180 min, much faster than the passive drug release as shown in **Figure 4B**. This result successfully demonstrated a stepwise triggered drug release from HCPT@HPBNs@PAA/PAH/HA-g-PEG upon NIR laser irradiation. It was likely attributed to the high autologous photothermal effect of PB, by which the temperature throughout the agent was significantly elevated, resulting in the accelerated dissolution of HCPT in the physiological fluids and the accelerated exchange rate between the internal space of the NPs and external solution environment, leading to the triggered drug release.

Investigation on active tumor targeting and circulation profile

To evaluate the active targeting to Hela cells in vitro, the cellular uptake of HPBNs@PAA/PAH/HA-g-PEG was investigated quantitatively in comparison with HPBNs@PAA/PAH/PEG (HA free nanoparticle) by measuring the intracellular iron contents using ICP-MS. As seen from **Figure 5A**, both of the two NPs were internalized by Hela cells in a concentration-dependent manner while the iron content in the Hela cells incubated with HPBNs@PAA/PAH/HA-g-PEG was obviously higher than that of HPBNsHPBNs@PAA/PAH/PEG incubated cells at all PB concentrations. The cellular uptake of the former was observed to be twice as much as the latter at the PB concentration of 100 μg/mL and 150μg/mL. It indicated the high-efficiency cancer cell targeting of HPBNs@PAA/PAH/HA-g-PEG. To confirm the cellular uptake of the HPBNs@PAA/PAH/HA-g-PEG is specific to CD44 receptor, competitive binding experiments were performed by incubating the Hela cells with HPBNs@PAA/PAH/HA-g-PEG in

the presence of excess amount of free HA. It was found that the presence of free HA did not change the cellular uptake of HPBNs@PAA/PAH/PEG, but significantly diminished the uptake of HPBNs@PAA/PAH/HA-g-PEG by Hela cell, probably attributed to the competitive binding of free HA to the CD44 receptor on Hela cells. The cellular uptake of HPBNs@PAA/PAH/HA-g-PEG was investigated in comparison with HPBNs@PAA/PAH/PEG using fluorescence microscopy after the label of the NPs with IRDye® 800 CW. Upon excitation by the light of 740 nm, both of the NPs exhibited red fluorescence. As shown in **Figure 5B**, after incubation for 4 h, Hela cells incubated with HPBNs@PAA/PAH/HA-g-PEG were significantly brighter than HPBNs@PAA/PAH/PEG incubated cells. This result indicated that, in comparison with HPBNs@PAA/PAH/PEG, HPBNs@PAA/PAH/HA-g-PEG can be internalized more efficiently by Hela cells through endocytosis. Thus, our data provided a strong evidence that HPBNs@PAA/PAH/HA-g-PEG can be internalized more efficiently by Hela cell through the CD44 receptor mediated active targeting.

The success to use HPBNs@PAA/PAH/HA-g-PEG for targeting Hela cells in vitro encouraged us to further explore its performance in vivo. After intravenously injection of IRdye 800CW labeled HPBNs@PAA/PAH/HA-g-PEG and HPBNs@PAA/PAH/PEG, fluorescence imaging of the mice was performed at different time interval for tracking the NPs in vivo. As shown in **Figure 5C**, the fluorescence signal was mainly observed in liver and spleen at 1 h post injection. Nevertheless, at 24 h post injection, the fluorescence signal in the tumor region of HPBNs@PAA/PAH/HA-g-PEG injected nude mouse was much higher than that of HPBNs@PAA/PAH/PEG injected mouse, suggesting the high efficiency of tumor targeting of HPBNs@PAA/PAH/HA-g-PEG. Fluorescence intensities of excised vital organs, blood and tumors were evaluated at 24 h post injection to further validate the tumor-targeting capability of the nanoagents (as shown in **Figure 5D**). The distribution of fluorescence intensity reflect that the HPBNs@PAA/PAH/PEG accumulated mainly in liver and couldn't effectively accumulate in the tumor. In contrast, the highest fluorescence intensity was observed in the tumor at 24 h for the HPBNs@PAA/PAH/HA-g-PEG injected mice. The effective tumor-targeting of HPBNs@PAA/PAH/HA-g-PEG was attributed to its suitable size and the active ligand of HA on the surface, which enable a perfect combination of CD44 receptor mediated active targeting and passive targeting by EPR effect. Moreover, the introduction of the PEG molecules could inhibit the agent from the removal by the RES, resulting a prolonged blood circulation time for tumor targeting. The excellent tumor-targeting capability of HPBNs@PAA/PAH/HA-g-PEG is favorable to in vivo cancer therapy.

The blood circulation parameters of HPBNs, HPBNs@PAA/PAH/PEG and HPBNs@PAA/PAH/HA-g-PEG were investigated by measuring the Fe content in blood via ICP measurement by intravenously administrated with the agent at the same PB dosage of 10mg/kg. Parameters including elimination half-life ($T_{1/2}$), mean residence time (MRT) and area under the plasma concentration-time curve from zero to time infinity ($AUC_{0-\infty}$) were evaluated using the KineticaTM soft-ware package (version 5.0, Thermo Fisher Scientific Inc., MA, USA). As seen in **Table 1**, the blood half-life, MRT and $AUC_{0-\infty}$ of HPBNs were calculated to be 5.6 h, 6.89 h and 398.42 h·mg/L. Due to the pegylation, HPBNs@PAA/PAH/PEG and HPBNs@PAA/PAH/HA-g-PEG displayed longer blood circulation time than HPBNs. $T_{1/2}$, MRT and $AUC_{0-\infty}$ were calculated to be 8.7 h, 9.84 h and 502.47 h·mg/L for HPBNs@PAA/PAH/PEG and 8.3 h, 9.67 h and 478.42 h·mg/L for HPBNs@PAA/PAH/HA-g-PEG. Thus, it provided evidence that HPBNs@PAA/PAH/PEG and HPBNs@PAA/PAH/HA-g-PEG can maintain long circulation time due to the introduction of PEG chains.

Table 1. Blood circulation parameters of HPBNs, HPBNs@PAA/PAH/PEG and HPBNs@PAA/PAH/HA-g-PEG.

Nanoparticles	Injection dose	Half-life	MRT	$AUC_{0-\infty}$
HPBNs	10mg/kg	5.6 h	6.89 h	398.42 h·mg/L
HPBNs@PAA/PAH/PEG	10mg/kg	8.7 h	9.84 h	502.47 h·mg/L
HPBNs@PAA/PAH/HA-g-PEG	10mg/kg	8.3 h	9.67 h	478.42 h·mg/L

In vitro photothermal cytotoxcities

The targeted killing effect on Hela cells was evaluated in term of the photothermal therapy using HPBNs@PAA/PAH/HA-g-PEG, chemotherapy using HCPT@HPBNs@PAA/PAH/HA-g-PEG and the combined thermochemotherapy using HCPT@HPBNs@PAA/PAH/HA-g-PEG and NIR laser irradiation in comparison with the HA free nanoagent, respectively. The biocompatibility of HPBNs@PAA/PAH/HA-g-PEG and HPBNs@PAA/PAH/PEG to Hela cells were evaluated before the investigation of their therapeutic potential. **Figure S3** revealed that both of them showed almost no toxicity to Hela cells even at the high concentration of 200 μg/mL, indicating their reliable biosafety.

To visualize the photothermal cytotoxcities, Hela cells were incubated with HPBNs@PAA/PAH/HA-g-PEG and HPBNs@PAA/PAH/PEG for 4 h, respectively. After washing with PBS buffer, Hela cells were irradiated by an 808 nm NIR laser at 1 W/cm^2 for 10 min. The treatments with agent only and laser only were also implemented as controls. Calcein AM and PI staining were used for assessment of cellular viability as shown in **Figure 6**. Upon treatment with either the agent or laser alone, Hela cells presented entire vivid green fluorescence, demonstrating the good survival of the cells. On the contrary, red fluorescence represented the death of Hela cells was observed upon treatment with both agents and laser. Upon laser irradiation, the Hela cells incubated with HPBNs@PAA/PAH/PEG showed a partial red fluorescence while the Hela cells incubated with HPBNs@PAA/PAH/HA-g-PEG exhibited an entire red fluorescence. It indicated that the introduction of HA targeting molecules into the nanoagent resulted in remarkably higher photothermal cytotoxcity at the same PB concentration.

Hela cells were incubated with HCPT@HPBNs@PAA/PAH/HA-g-PEG, HCPT@HPBNs@PAA/PAH/PEG and free HCPT at various drug concentrations for 48 and 72 h, respectively. As shown in **Figure 7A**, the IC50 values of the HCPT@HPBNs@PAA/PAH/HA-g-PEG treated Hela cells were evaluated to be 500 nM for 48 h and 161 nM for 72 h, significantly lower than that of HCPT@HPBNs@PAA/PAH/PEG (1363 nM for 48 h and 892 nM for 72 h) and free HCPT (1450 nM for 48 h and 987 nM for 72 h), respectively. The increased chemocytotoxicity was attributed to the CD44 receptor mediated high-efficient uptake of the HA modified nanoagent.

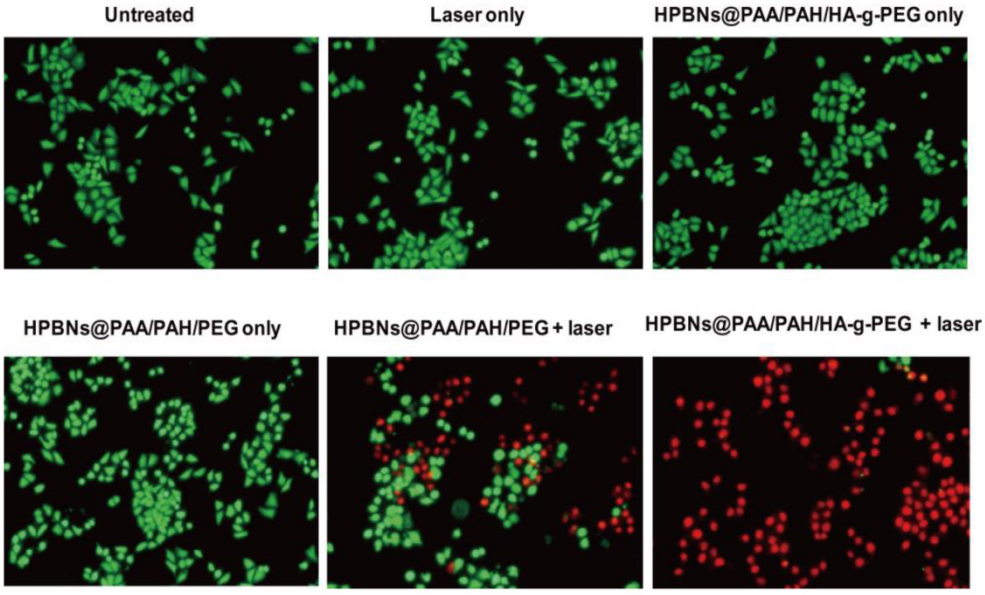

Figure 6. Fluorescence microscopy images of Hela cells stained with calcein AM and PI upon different treatments.

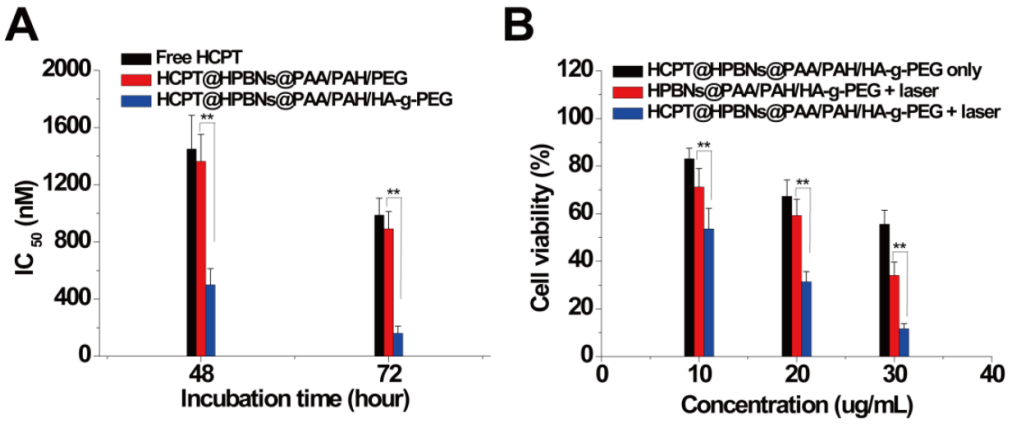

Figure 7. (A) IC50 of Hela cells after treating with free HCPT and the HCPT loaded nanoagents. (B) Viability of Hela cells determined by MTT method after treating with HCPT@HPBNs@PAA/PAH/HA-g-PEG only, HPBNs@PAA/PAH/HA-g-PEG + laser and HCPT@HPBNs@PAA/PAH/HA-g-PEG + laser. *: $p < 0.05$ and **: $p < 0.01$.

To investigate the in vitro synergetic effect of photothermal therapy and chemotherapy using HCPT@HPBNs@PAA/PAH/HA-g-PEG, MTT assay was used to evaluate the cellular viabilities at 24 h after the treatments with the HCPT loaded (or free) agents at different concentrations with or without laser irradiation. As seen from **Figure 7B**, all of the therapies showed an increasing inhibition rate against Hela cells in a dose-dependent manner. At the highest dosage, the cellular viability decreased to 55.6 % for HCPT@HPBNs@PAA/PAH/HA-g-PEG only (HCPT concentration: 3 μg/mL), 34.1% for HPBNs@PAA/PAH/HA-g-PEG + laser and 11.67 % for HCPT@HPBNs@PAA/PAH/HA-g-PEG (HCPT concentration: 3 μg/mL) + laser. These results demonstrated that the combination of chemotherapy and photothermal therapy through HCPT@HPBNs@PAA/PAH/HA-g-PEG could significantly improve the potential for target cancer cell killing compared with either therapy alone.

In vivo tumor therapy

In vivo tumor therapy was investigated on Hela tumor-bearing nude mice. Eight groups of mice with average tumor size of 100 mm^3 were treated with saline only, laser only, HPBNs@PAA/PAH/PEG only, HPBNs@PAA/PAH/HA-g-PEG only, HCPT@HPBNs@PAA/PAH/HA-g-PEG only, HPBNs@PAA/PAH/PEG + laser, HPBNs@PAA/PAH/HA-g-PEG + laser, HCPT@HPBNs@PAA/PAH/HA-g-PEG + laser, respectively. According to the result of NIR fluorescent tracking study, laser irradiation was performed at 24 h after the intravenous injection of different agents at the dose of 10 mg/kg, ensuring the high accumulation of the nanoagents in tumor tissue.

During the laser treatment, temperature changes in the tumor region were acquired by both infrared thermal imager and thermometer. As seen from **Figure 8A and Figure S4** , compared with the constant tumor temperature (37.1 °C) in saline treated nude mouse, the temperature of tumor increased to 43.0 °C and 53 °C for the HPBNs@PAA/PAH/PEG and HPBNs@PAA/PAH/HA-g-PEG injected nude mice under NIR laser exposure, respectively. The higher elevated tumor temperature in the HPBNs@PAA/PAH/HA-g-PEG treated nude mouse indicated that HPBNs@PAA/PAH/HA-g-PEG could accumulate in the tumor by the high-efficient active tumor targeting and the temperature was high enough to ablate tumors in vivo.

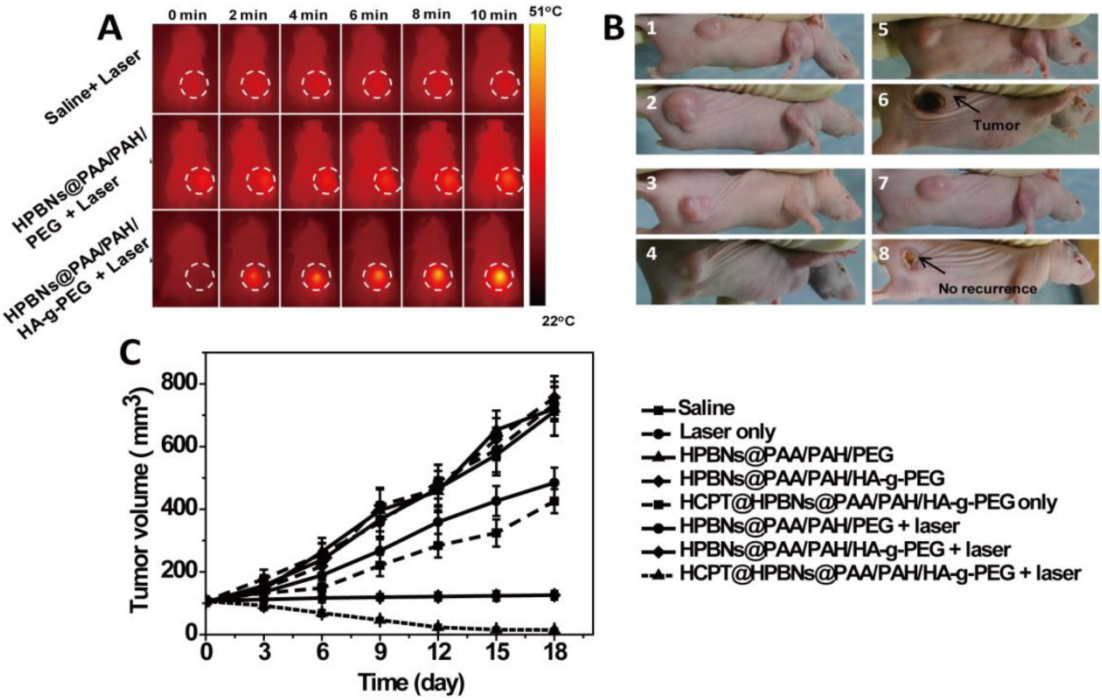

Figure 8. (A) IR thermal images of Hela tumor-bear mice at different time intervals under the 808-nm laser irradiation (0.8 W/cm^2). (B) The representative tumor photographs of each group were recorded before and after treatment: (1) saline group before therapy; (2) saline group at 18 day after therapy, (3) HCPT@ HPBNs@PAA/PAH/HA-g-PEG group before therapy; (4) HCPT@ HPBNs@PAA/PAH/HA-g-PEG group at 18 day after therapy, (5) HPBNs@PAA/PAH/HA-g-PEG + laser group before therapy; (6) HPBNs@PAA/PAH/HA-g-PEG + laser group at 18 day after therapy, (7) HCPT@HPBNs@PAA/PAH/HA-g-PEG + laser group before therapy; (8) HCPT@HPBNs@PAA/PAH/HA-g-PEG + laser group at 18 day after therapy. (C) The growth of Hela tumors in nude mice after various treatments.

Both tumor photographs and tumor volume were measured to evaluate the corresponding therapeutic outcome after different treatments (**Figure 8B and 8C**). It was found that the tumors grew at a similar growth rate and tumor volume increased rapidly from original 100 mm^3 to approximately 750 mm^3 within 18 days in the mice treated with saline only, HPBNs@PAA/PAH/HA-g-PEG only, HPBNs@PAA/PAH/PEG only and laser only. These results indicated that laser irradiation or the HCPT free agents alone at the experimental condition did not cause potential destructive effects. Compared with the saline only group, it is obvious that the tumor growth was inhibited to different extent in the agent + laser groups and the HCPT@HPBNs@PAA/PAH/HA-g-PEG only group. The tumor size in the HPBNs@PAA/PAH/PEG+laser group increased to about 473 mm^3, suggesting an insufficient hyperpyrexia for ablating tumor due to the lower accumulation of HPBNs@PAA/PAH/PEG in tumor tissue through a passive targeting. Nevertheless, the tumor size of mice treated with HPBNs@PAA/PAH/HA-g-PEG in combination of laser irradiation almost kept constant at about 100mm^3 within 18 days, implying an efficient photothermal ablation effect to inhibit tumor growth because of the greatly improved uptake of HCPT@HPBNs@PAA/PAH/HA-g-PEG by tumor cells through an active-targeting. As expected, the tumor growth was inhibited in the mice treated with HCPT@HPBNs@PAA/PAH/HA-g-PEG only and the tumor size was 413 mm^3. More excitingly, the tumor size decreased rapidly from original 100 mm^3 to 15 mm^3 within 18 day after the treatment with HCPT@HPBNs@PAA/PAH/HA-g-PEG in combination of laser irradiation. These results demonstrated that the combined thermochemotherapy was more cytotoxic to tumor cells than the PTT treatment or the chemotherapy alone. The main cause of the synergistic thermochemotherapy is as follows: Firstly, the photothermal effect can greatly enhance the sensitivity of the cancer cells toward anti-cancer drug, resulting in the improved drug efficacy. In addition, the photothermal effect can also trigger a rapid drug release to achieve a high effective drug concentration in the tumor. Therefore, HCPT@HPBNs@PAA/PAH/HA-g-PEG could be operated as a powerful thermochemotherapy agent for in-vivo therapy of cancer.

3.7 Toxicology

The in vivo toxicity of HCPT@HPBNs@PAA/PAH/HA-g-PEG was evaluated in term of body weight change, histological examination and serum biochemistry assays on health nude mice after the injection of HCPT@HPBNs@PAA/PAH/HA-g-PEG at a dose of 10mg/kg, which was equal to the therapy dose. Compared with untreated mice, no significant body weight loss and apparent histological injury were observed in HCPT@HPBNs-HA-PEG injected mice (**Figure 9A and 9B**). Serum biochemistry assay results showed that hematological parameters including white blood cells (WBC), red blood cells (RBC), platelets (PLT) and neutrophile granulocyte (GRN) in HCPT@HPBNs@PAA/PAH/HA-g-PEG injected mice nearly have no change compared with untreated nude mice (**Table 2**). Overall preliminary results confirmed that HCPT@HPBNs@PAA/PAH/HA-g-PEG was not noticeably toxic to nude mice, suggesting the security for medical applications.

Table 2. Blood biochemical indexes.

	Untreated mice	HCPT@HPBNs@PAA/PAH/HA-g-PEG injected mice (10 mg/kg)		
		1 day	7day	30 day
WBC (10^9/L)	12.26 ± 2.37	12.99 ± 1.91	12.88 ± 1.21	11.96 ± 1.44
RBC (10^{12}/L)	9.467 ± 2.55	8.97 ± 1.49	9.98 ± 1.94	9.21 ± 1.14
PLT (10^{12}/L)	0.65 ± 0.14	0.61 ± 0.12	0.63 ± 0.09	0.67 ± 0.13
GRN (10^9/L)	4.21 ± 0.53	4.64 ± 0.72	4.34 ± 0.48	4.70 ± 0.25

Conclusions

A well-designed multifunctional nanoagent of HCPT@HPBNs@PAA/PAH/HA-g-PEG has been successfully constructed by integrating different components including hollow PB nanoparticle as photothermal agent and drug carrier, HCPT as chemotherapeutic agent, and HA-g-PEG as capping agent for prolonged blood circulation time and CD44 receptor mediated tumor targeting into one single agent. In vitro cellular uptake and in vivo NIR fluorescence imaging confirmed that HCPT@HPBNs@PAA/PAH/HA-g-PEG held a great potential for tumor-specific targeting. Under the irradiation of NIR laser, HCPT@HPBNs@PAA/PAH/HA-g-PEG exhibited excellent photothermal efficiency and light triggered drug release, resulting in significantly high inhibition effect on cancer cells. Both in vitro and in vivo experiments showed that the combination of chemotherapy and photothermal therapy through HCPT@HPBNs@PAA/PAH/HA-g-PEG could offer a synergistically improved therapeutic efficacy compared with either therapy alone. In addition, PB nanoparticles and their derivatives have been reported to be contrast agents to enhance photoacoustic imaging and multimodal imaging. Therefore, the obtained nanoagent could operate as a very promising theranostic nanomedicine to be capable of noninvasive imaging and remote-controlled therapy.

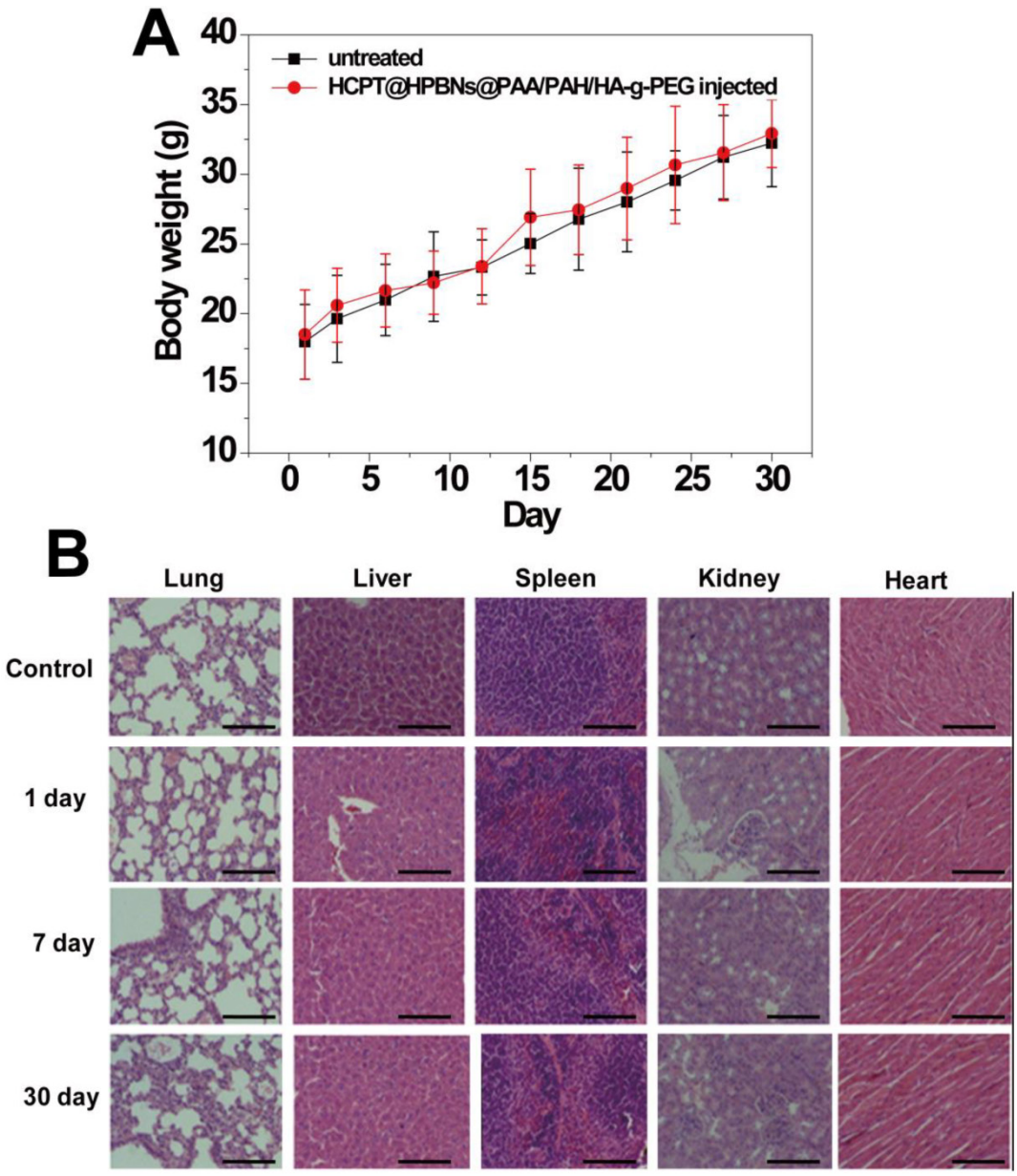

Figure 9. (A) Body weight curves of the mice for 30 days with or without a single intravenous injection of HCPT@HPBNs@PAA/PAH/HA-g-PEG at the dosage of 10 mg/kg. (B) Histological examination for mice treated with HCPT@HPBNs@PAA/PAH/HA-g-PEG at the dose of 10 mg/kg. Untreated healthy mice were used as the control. Scale bar = 50 μm.

Supplementary Material

Figures S1- S4.
http://www.thno.org/v06p0040s1.pdf

Acknowledgements

This work was financially supported by National Natural Science Foundation of China (Grant No. 21273014 and No. 81201186), National Natural Science Foundation for Distinguished Young Scholars (Grant No. 81225011), State Key Program of National Natural Science of China (Grant No. 81230036) and the Foundation for Innovative Research Groups of the National Natural Science Foundation of China (Grant No.81421004).

Competing Interests

The authors have declared that no competing interest exists.

References

1. Chung MF, Chen KJ, Liang HF, Liao ZX, Chia WT, Xia Y, Sung HW. A new liposomal system capable of generating CO_2 bubbles to induce transient cavitation, lysosomal rupturing, and cell necrosis. Angew Chem Int Ed Engl. 2012; 51: 10089-93.
2. Bao G, Mitragotri S, Tong S. Multifunctional nanoparticles for drug delivery and molecular imaging. Annu Rev Biomed Eng. 2013;15:253-82
3. Zhang L, Gu FX, Chan JM, Wang AZ, Langer RS, Farokhzad OC. Nanoparticles in medicine: therapeutic applications and developments. Clin Pharmacol Ther. 2008; 83: 761-9.

4. Kolishetti N, Dhar S, Valencia PM, Lin LQ, Karnik R, Lippard SJ, Langer R, Farokhzad OC. Engineering of self-assembled nanoparticle platform for precisely controlled combination drug therapy. Proc Natl Acad Sci USA. 2010; 107: 17939-44.
5. Zhang L, Chan JM, Gu FX, Rhee JW, Wang AZ, Radovic-Moreno AF, Alexis F, Langer R, Farokhzad OC. Self-assembled lipidpolymer hybrid nanoparticles: a robust drug delivery platform. ACS Nano. 2008; 2: 1696-702.
6. Chan JM, Rhee JW, Drum CL, Bronson RT, Golomb G, Langer R, Farokhzad OC. In vivo prevention of arterial restenosis with paclitaxel-encapsulated targeted lipid-polymeric nanoparticles. Proc Natl Acad Sci USA. 2011; 108: 19347-52.
7. Liang XL, Gao J, Jiang LD, Luo JW, Jing LJ, Li XD, Jin YS, Dai ZF. Nanohybrid liposomal cerasomes with good physiological stability and rapid temperature responsiveness for HIFU triggered local chemotherapy of cancer. ACS Nano 2015; 9: 1280-93.
8. Ma Y, Liang XL, Tong S, Bao G, Ren QS, Dai ZF. Gold nanoshell nanomicelles for potential magnetic resonance imaging, light-triggered drug release, and photothermal therapy. Adv Funct Mater. 2012; 23: 815-22.
9. Jing LJ, Liang XL, Li XD, Lin L, Yang YB, Yue XL, Dai ZF. Mn-porphyrin conjugated Au nanoshells encapsulating doxorubicin for potential magnetic resonance imaging and light triggered synergistic therapy of cancer. Theranostics. 2014; 4:858-71
10. Jin YS, Wang JR, Ke HT, Wang SM, Dai ZF. Graphene oxide modified PLA microcapsules containing gold nanoparticles for ultrasonic/CT bimodal imaging guided photothermal tumor therapy. Biomaterials. 2013, 34: 4794-802.
11. Guo CX, Jin YS, Dai ZF. Multifunctional ultrasound contrast agents for imaging guided photothermal therapy. Bioconjug Chem. 2014, 25 (5): 840-54.
12. Sheng ZH, Hu DH, Zheng MB, Zhao PF, Liu HL, Gao DY, Gong P, Gao GH, Zhang PF, Ma YF, Cai LT. Smart human serum albumin-indocyanine green nanoparticles generated by programmed assembly for dual-modal imaging-guided cancer synergistic phototherapy. ACS Nano. 2014; 8: 12310-22.
13. Sun X, Huang X, Yan X, Wang Y, Guo J, Jacobson O, Liu D, Szajek L, Zhu W, Niu G, Kiesewetter DO, Sun S, Chen X. Chelator-free ^{64}Cu integrated Au nanomaterials for positron emission tomography imaging guided photothermal cancer therapy. ACS Nano. 2014; 8: 8438-46.
14. Yang K, Xu H, Cheng L, Sun C, Wang J, Liu Z. In vitro and in vivo near-infrared photothermal therapy of cancer using polypyrrole organic nanoparticles. Adv Mater. 2012; 24: 5586-92.
15. Huang P, Omar P, Wang X, Wang Z, Li Z, Zhang CL, Chen F, Jing L, Cui D, Chen X. Chiral guanosine 5'-monophosphate-capped gold nanoflowers: controllable synthesis, characterization, surface-enhanced raman scattering activity, cellular imaging and photothermal therapy. Nano Res. 2012; 5: 630-9.
16. Park H, Yang J, Lee J, Haam S, Choi IH, Yoo KH. Multifunctional nanoparticles for combined doxorubicin and photothermal treatments. ACS Nano. 2009; 3: 2919–26.
17. Huschka R, Barhoumi A, Liu Q, Roth JA, Ji L, Halas NJ. Gene silencing by gold nanoshell-mediated delivery and laser-triggered release of antisense oligonucleotide and siRNA. ACS Nano. 2012; 6: 7681-91.
18. Xiao ZY, Ji CW, Shi JJ, Pridgen EM, Frieder J, Wu J, Farokhzad OC. DNA self-assembly of targeted near-infrared-responsive gold nanoparticles for cancer thermo-chemotherapy. Angew Chem Int Ed Engl. 2012; 51: 11853-57.
19. Hribar KC, Lee MH, Lee D, Burdick JA. Enhanced release of small molecules from near-infrared light responsive polymer-nanorod composites. ACS Nano. 2011; 5: 2948-56.
20. Skrabalak SE, Chen J, Sun Y, Lu X, Au L, Cobley CM, Xia Y. Gold nanocages: synthesis, properties, and applications. Acc Chem Res. 2008; 41: 1587-95.
21. Sun TM, Du JZ, Yao YD, Mao CQ, Dou S, Huang SY, Zhang PZ, Leong KW, Song EW, Wang J. Simultaneous delivery of siRNA and paclitaxel via a "Twoin-One" micelleplex promotes synergistic tumor suppression. ACS Nano. 2011; 5: 1483-94.
22. Sherlock SP, Tabakman SM, Xie LM, Dai HJ. Photothermally enhanced drug delivery by ultrasmall multifunctional FeCo/graphitic shell nanocrystals. ACS Nano. 2011; 5: 1505-12.
23. Lee SM, Park H, Choi JW, Park YN, Yun CO, Yoo KH. Multifunctional nanoparticles for targeted chemophotothermal treatment of cancer cells. Angew Chem Int Ed Engl. 2011; 50: 7581-86.
24. Sherlock S, Dai H. Multifunctional FeCo-graphitic carbon nanocrystals for combined imaging, drug delivery and tumor-specific photothermal therapy in mice. Nano Res. 2011; 4: 1248-60.
25. Peng JR, Qi TT, Liao JF, Chu B. Y, Yang Q, Qu Y, Li WT, Li, H, Luo F, Qian ZY. Mesoporous magnetic gold "nanoclusters" as theranostic carrier for chemo-photothermal co-therapy of breast cancer. Theranostics. 2014; 4: 678-92.
26. Xia YN, Li WY, Cobley CM, Chen JY, Xia XH, Zhang Q, Yang MX, Cho EC, Brown PK. Gold nanocages: from synthesis to theranostic applications. Acc Chem Res. 2011; 44: 914-24.
27. Cobley CM, Au L, Chen J, Xia Y. Targeting gold nanocages to cancer cells for photothermal destruction and drug delivery. Expert Opin Drug Deliv. 2010; 7: 577-87.
28. Ke HT, Wang JR, Dai ZF, Jin YS, Qu EZ, Xing ZW, Liu JB. Gold-nanoshelled microcapsules: a theranostic agent for ultrasound contrast imaging and photothermal therapy. Angew Chem Int Ed Engl. 2011; 50: 3017-21.
29. Ke HT, Wang JR, Tong S, Jin YS, Wang SM, Qu EZ, Bao G, Dai ZF. Gold nanoshelled liquid perfluorocarbon magnetic nanocapsules: a nanotheranostic platform for bimodal ultrasound/magnetic resonance imaging guided photothermal tumor ablation. Theranostics. 2014; 4: 12-23.
30. Yi DK, Sun IC, Ryu JH, Koo H, Park CW, Youn IC, Choi K, Kwon IC, Kim K, Ahn CH. Matrix metalloproteinase sensitive gold nanorod for simultaneous bioimaging and photothermal therapy of cancer. Bioconjug Chem. 2010; 21: 2173-77.
31. Wang CH, Huang YJ, Chang CW, Hsu WM, Peng CA. In vitro photothermal destruction of neuroblastoma cells using carbon nanotubes conjugated with GD2 monoclonal antibody. Nanotechnology. 2009; 20: 315101.
32. Zhou F, Xing D, Ou Z, Wu B, Resasco DE, Chen WR. Cancer photothermal therapy in the near-infrared region by using single-walled carbon nanotubes. J Biomed Opt. 2009; 14: 021009.
33. Qin XC, Guo ZY, Liu ZM, Zhang W, Wan MM, Yang BW. Folic acid-conjugated graphene oxide for cancer targeted chemo-photothermal therapy. J Photochem Photobiol B. 2013; 120: 156-62.
34. Yang K, Hu L, Ma X, Ye S, Cheng L, Shi X, Li C, Li Y, Liu Z. Multimodal imaging guided photothermal therapy using functionalized graphene nanosheets anchored with magnetic nanoparticles. Adv Mater. 2012; 24: 1868-72.
35. Lee SM, Park H, Yoo KH. Synergistic cancer therapeutic effects of locally delivered drug and heat using multifunctional nanoparticles. Adv Mater. 2010; 22: 4049-53.
36. Yang J, Choi J, Bang D, Kim E, Lim EK, Park H, Suh JS, Lee K, Yoo KH, Kim EK, Huh YM, Haam S. Convertible organic nanoparticles for near-infrared photothermal ablation of cancer cells. Angew Chem Int Ed Engl. 2011; 50: 441-4.
37. Fu GL, Liu W, Feng SS, Yue XL. Prussian Blue Nanoparticles operate as a new generation of photothermal ablation agents for cancer therapy. Chem Commun (Camb). 2012; 48: 11567-69.
38. Fu GL, Liu W, Li YY, Jin YS, Jiang LD, Liang XL, Feng SS, Dai ZF. Magnetic Prussian blue nanoparticles for targeted photothermal therapy under magnetic resonance imaging guidance. Bioconjug Chem. 2014, 25:1655-63.
39. Jing LJ, Liang XL, Deng ZJ, Feng SS, Li XD, Huang MM, Dai ZF. Prussian blue coated gold nanoparticles for simultaneous photoacoustic/CT bimodal imaging and photothermal ablation of cancer. Biomaterials. 2014; 35: 5814-21.
40. Cheng L, Gong H, Zhu WW, Liu JJ, Wang XY, Liu G, Liu Z. PEGylated Prussian blue nanocubes as a theranostic agent for simultaneous cancer imaging and photothermal therapy. Biomaterials. 2014; 35: 9984-52.
41. Cai XJ, Jia XQ, Gao W, Zhang K, Ma M, Wang SG, Zheng YY, Shi JL, Chen HR. Aversatile nanotheranostic agent for efficient dual-mode imaging guided synergistic chemo-thermal tumor therapy. Adv Funct Mater. 2015; 25: 2520–2529.
42. Wu M, Wang QT, Liu XL, Liu JF. Highly efficient loading of doxorubicin in Prussian Blue nanocages for combined photothermal/chemotherapy against hepatocellular carcinoma. RSC Adv. 2015; 5: 30970-30980.
43 Hsiang, YH, Hertzberg R, .Hecht S, Liu LF. Camptothecin induces protein-linked DNA breaks via mammalian DNA topoisomerase I. J Biol Chem. 1985; 260: 14873–14878.
44. Yu M, Jambhrunkar S, Thorn P, Chen J, Gu W, Yu C. Hyaluronic acid modified mesoporous silica nanoparticles for targeted drug delivery to CD44- overexpressing cancer cells. Nanoscale. 2013; 5: 178-83.
45. Toole BP, Wight TN, Tammi MI. Hyaluronan-cell interactions in cancer and vascular disease. J Biol Chem. 2002; 277: 4593-6.
46. Lee T, Lim EK, Lee J, Kang B, Choi J, Park HS, Suh JS, Huh YM, Haam S. Efficient CD44-targetedmagnetic resonance imaging (MRI) of breast cancer cells using hyaluronic acid (HA)-modified $MnFe_2O4$ nanocrystals. Nanoscale Res Lett. 2013; 8: 1-9.
47. Lee DE, Kim AY, Saravanakumar G, Koo H, Kwon IC, Choi K, Park JH, Kim K. Hyaluronidase-sensitive SPIONs for MR/optical dual imaging nanoprobes. Macromol Res. 2011; 19: 861-7.
48. Wei X, Senanayake TH, Warren G, Vinogradov SV. Hyaluronic acid-based nanogel-drug conjugates with enhanced anticancer activity designed for the targeting of CD44-positive and drug-resistant tumors. Bioconjug Chem. 2013; 24: 658-68.
49 Li JC, He Y, Sun WJ, Luo Y, Cai HD, Pan YQ, Shen MW, Xia JD, Shi XY. Hyaluronic acid-modified hydrothermally synthesized iron oxide nanoparticles for targeted tumor MR imaging. Biomaterials. 2014; 35: 3666-77.
50. Hu M, Furukawa S, Ohtani R, Sukegawa H, Nemot Y, Reboul J, Kitagawa S, Yamauchi Y. Synthesis of Prussian blue nanoparticles with a hollow interior by controlled chemical etching. Angew Chem Int Ed Engl. 2012; 51: 984-8.